Nuclear Instruments and Methods in Physics Research A 367 (1995) 316-320

ELSEVIER

NUCLEAR INSTRUMENTS & METHODS IN PHYSICS RESEARCH Section A

Construction update and drift velocity calibration for the CLAS drift chamber system

M.D. Mestayer[a,*], F.J. Barbosa[a], P. Bonneau[a], E. Burtin[d], S. Christo[a], G. Doolittle[a], S.A. Dytman[h], G.P. Gilfoyle[g], C.E. Hyde-Wright[c], A. Klein[c], M.V. Kossov[f], S.E. Kuhn[c], R. Magahiz[b], R.A. Miskimen[i], L.Y. Murphy[e], J.E. O'Meara[a], T.D. Pyron[c], L. Qin[c], B.A. Raue[c], R.A. Schumacher[b], W. Tuzel[a], L.B. Weinstein[a], A. Yegneswaran[a]

[a] *CEBAF, Newport News, VA, USA*
[b] *Carnegie-Mellon University, Pittsburgh, PA, USA*
[c] *Old Dominion University, Norfolk, VA, USA*
[d] *University of South Carolina, Columbia, SC, USA*
[e] *CE Saclay, Gif sur Yvette, France*
[f] *Christopher Newport University, Newport News, VA, USA*
[g] *University of Richmond, Richmond, VA, USA*
[h] *University of Pittsburg, Pittsburg, PA, USA*
[i] *University of Massachussetts, Amherst, MA, USA*

Abstract

We briefly describe the drift chamber system for the CLAS detector at CEBAF, concentrating on the method which will be used to calibrate the drift velocity function. We identify key features of the function which should apply to any small-cell drift chamber geometry in which the cathode and anode surfaces are wires. Using these ideas, we describe a simple method to compensate for variations in the drift velocity function due to environmental changes.

1. CLAS drift chamber overview

One of the experimental halls at CEBAF will house a large acceptance particle detector (CLAS) [1] based upon a six-coil toroidal magnet. The drift chambers have an unusual geometry and have been an interesting challenge to design, build and instrument. They were described at the 1992 Wire Chamber Conference [2] and will only be briefly reviewed in this article.

There are three types of drift chamber in the CLAS detector. "Region 1" chambers surround the target in a region of low magnetic field. The "Region 2" chambers are somewhat larger and are situated between the magnet coils in a region of high field, while the "Region 3" chambers are large devices located radially outward of the magnet.

A full-sized prototype of the Region 1 six-sector assembly has been constructed. Fig. 1 displays the assembled structure as it will appear when installed.

The height of the assembly is approximately 2 m, with the longest wire being 70 cm. In order to minimize the amount of material which particles must traverse, we designed the chambers to have compressional members ("posts") which are removable. Individual chambers are strung with the post compression balancing the wire tension. Once all six chambers are strung, they are placed into the six-sector assembly and connected to neighboring chambers via short "struts". The posts are then removed, and the wire tension is borne by tension in the chamber-to-chamber struts. The assembly of the structure verified the practicality of the design concept. Each of the individual chambers in the assembly was strung with thick wires which mimicked the final tension of the strung chamber. After removal of the posts the tensions in the wires changed by less than 20%, verifying the tension-transfer design.

The Region 2 chambers are located between the coils of the toroidal magnet in the high-field region. To avoid large eddy-current forces during a possible magnet quench, the Region 2 endplates are made of a non-conducting fiberglass composite. In order to insure that the chambers are fully efficient for all charged tracks which do not hit the toroid coils, the thickness of endplate and electronics was kept as small as possible. Fig. 2 shows a cut through the endplate and toroidal coil showing details of the wire affixment and chamber-to-coil attachment. Note that the wires touch metal feedthroughs on their inner radii. The feedthroughs fit directly into precision holes drilled into the fiberglass endplate

* Corresponding author. E-mail mestayer@cebaf.gov

SSDI 0168-9002(95)00745-8

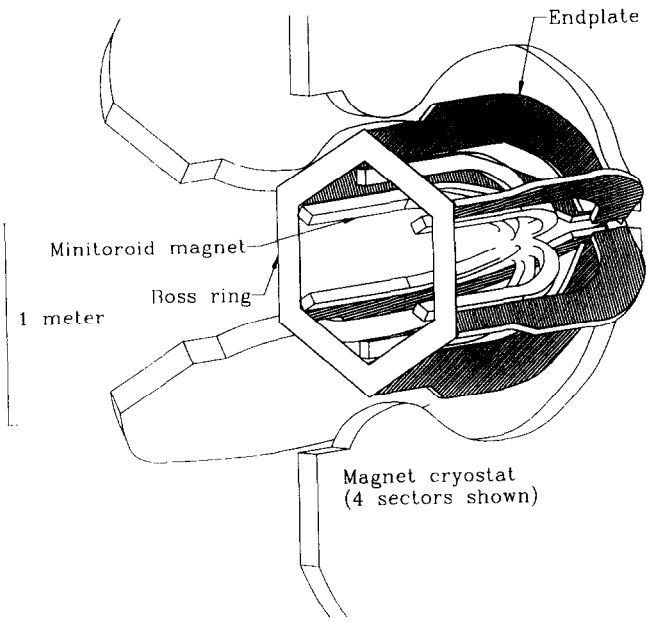

Fig. 1. Region 1 six-sector assembly.

body. This scheme is simple, inexpensive and provides sufficient accuracy in wire placement ($\approx 50\ \mu$m). We have verified that a prototype chamber with this type of feedthrough operates normally. Note also in Fig. 2 the spring attachment between endplate and magnet cryostat. These springs transfer the wire tension load from the endplates to the cryostat, while allowing motion of the cryostat of up to 3 mm without over-stressing the wires.

There has been substantial progress on the construction of the large Region 3 chambers. Two of the six chambers have been completely strung. A prototype chamber containing 192 sense wires has been operational since March 1994. We plan to run the prototype chamber continuously until turn-on of the CLAS detector in September 1996, thus providing an early warning if any operational problems develop. We have also used the prototype to establish operating conditions and

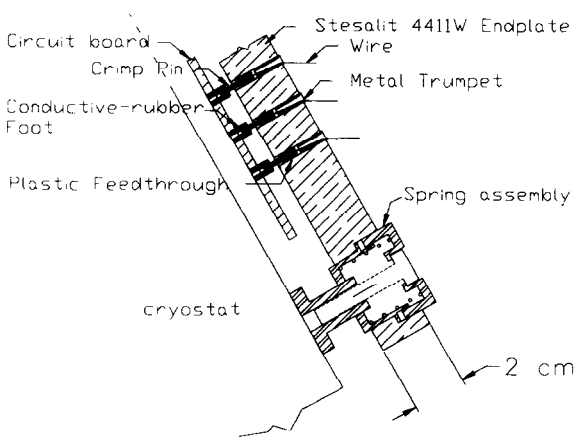

Fig. 2. Region 2: View of cut through end-plate and cryostat.

to develop calibration procedures, which we now discuss.

2. Calibration strategies

The various calibrations planned for the CLAS drift chambers include the following:

- Geometrical surveys: Using a combination of optical surveys and dedicated calibration runs (e.g. $\boldsymbol{B} = 0$, point target, cosmic ray runs, etc.) we will determine the position and orientation of the 18 separate drift chambers (three in each sector).

- Event time calibrations: Using a pulser system, we will pulse the on-chamber pre-amplifiers to check for dead wires as well as for changes in electronic delays, time-walk, etc.

- Drift velocity calibration: The drift velocity function can change with changing environmental conditions, e.g. pressure, temperature, gas mixture. A combination of internal consistency checks based upon track fitting and a laser pulsing system will allow us to measure key parameters of the drift velocity function.

We will discuss only the drift velocity calibration procedure in the remainder of this article.

2.1. Experimental setup

This study was done with the Region 3 prototype chamber in a cosmic-ray telescope. The prototype contains 192 sense wires, instead of the 2304 sense wires of an actual chamber, but in other aspects of construction and on-board instrumentation, is the same. The chamber has a hexagonal wire arrangement, with sense wires grouped into two six-layer superlayers. We fit cosmic ray tracks by minimiz-

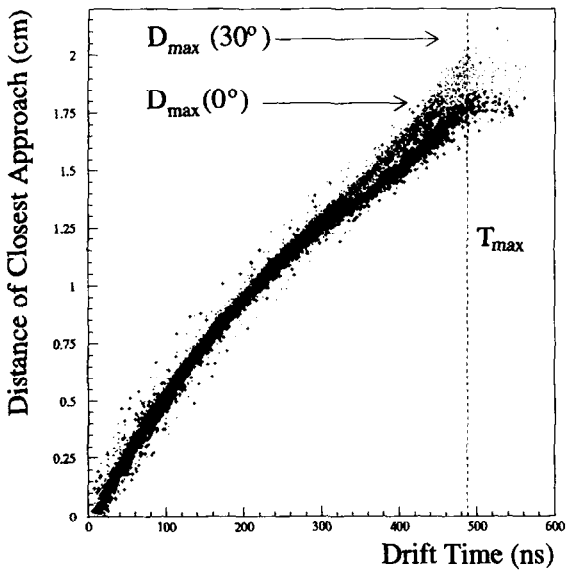

Fig. 3. D (cm) vs. T (ns) for wires not used in fit.

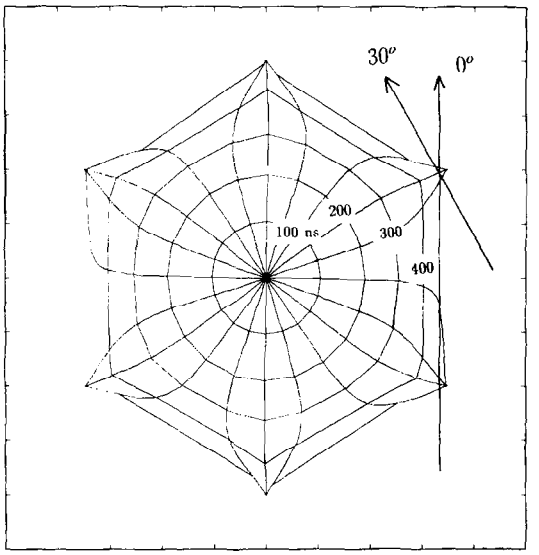

Fig. 4. Drift lines and drift isochrones (100 ns contours): Region 3 cell.

ing the residual between the calculated distance-of-closest-approach (D) of the track to a wire with the distance from the wire as calculated from its time (T) alone. In Fig. 3 we plot D vs. T for wires from one particular layer which was excluded from the track fit. The resulting scatterplot is the familiar drift velocity function.

2.2. General properties of the D vs. T correlation

On Fig. 3 we have indicated the maximum possible drift distance (D_{max}) as well as the corresponding time, T_{max}. Shown as different symbols are data points from tracks with entrance angle of 25–30°, and those with angle of 0–5°. Clearly, there is a track angle dependence to the D–T correlation. However, note that the two data samples seem to be characterized by the *same* value of T_{max}.

To understand this effect physically, we present in Fig. 4 a plot of isochrones for the cell in question, calculated using the program, GARFIELD [3]. Near the wire, the isochrones are circular, indicating that the D–T function is independent of track angle. Further from the wire the isochrones become non-circular, showing track angle dependence. Near the outer edges of the cell the isochrones become hyperboloid. This implies that the first-arriving ions from tracks which are near the periphery of the cell come from the high-field region near the field wire regardless of the location of the point at which the track is closest to the wire. This is the reason that the *same* value of T_{max} applies to tracks of any angle. For example, the two tracks shown (at 0° and 30°) have different distances of closest approach but give the same value for the time of the first arriving drift electron.

Looking again at Fig. 3, we note two other features of the data. First, the slope at small values of time is approximately equal to the slope at maximum time (T_{max}) [4] . Second, an inflection point (which corresponds to a minimum in the drift velocity) occurs at a distance of ≈0.615 of the maximum distance.

These constraints led us to a polynomial expression for the D vs. T function with only three adjustable parameters, V_0 (the saturated drift velocity), T_{smear} (the time smearing for tracks near the wires due to discrete ionization), and T_{max} (the maximum drift time). The quantities V_0 and T_{smear} are roughly constant, thus when some operating condition varies (like atmospheric pressure), we can characterize the change in the drift velocity with one parameter, T_{max}.

2.3. Derivation of the function

We now investigate the functional form for the dependence of D on time. The function also depends on θ, the track entrance angle. For brevity, we derive the function for the case of $\theta = 30°$, i.e. where the track is perpendicular to a line joining sense and field wire.

For simplicity, we assumed a simple three-power form, the first term of which is linear.

$$D = V_0 T + b\left(\left(\frac{T}{T_{max}}\right)^n + c\left(\frac{T}{T_{max}}\right)^m\right),$$

where V_0 is the value for the saturated drift velocity near $T = 0$, and T_{max} is the maximum drift time.

The first constraint is that the drift velocity near the sense wire ($T = 0$) is equal to the drift velocity near the field wire ($T = T_{max}$). Even though the field wire's local electric field at some particular distance is half that for the sense wire, the local drift velocities are approximately equal because this is in the high electric field region where drift velocities saturate. Therefore:

$$\frac{dD}{dT}(T = 0) = \frac{dD}{dT}(T = T_{max})$$

or

$$V_0 = V_0 + b(n + cm).$$

Thus

$$c = -n/m.$$

The second constraint is that the drift velocity reaches a minimum at the point of minimum electric field strength. Along a line from sense to field wire, we determined that the electric field reaches a minimum at approximately 0.615 of the distance from sense to field wire, using the GARFIELD program. The number 0.615 is characteristic of an infinite grid of hexagonal cells which our chambers approximate. It does not depend on cell size or voltage. In terms of drift time, this inflection point occurs at $T \approx 0.605T_{\max}$, for our particular running conditions. The value 0.605 is not a geometrical constant but is approximately constant for our choice of operating voltage. Therefore,

$$\frac{d^2D}{dT^2}(T = 0.605T_{\max}) = 0.$$

So

$$n(n-1)(0.605)^n = cm(m-1)(0.605)^m.$$

Substituting $c = -n/m$ yields

$$(n-1)(0.605)^n = (m-1)(0.605)^m.$$

Graphically we determined that the equation

$$n = 2.85 - 0.65(m-3)^{0.7}$$

describes the solution set. Using this relation between n and m, we were able to fit the D vs. T data to the functional form to obtain $n = 2$ and $m = 4.5$ as the exponents which best fit the data. To obtain good agreement with data, it was also necessary to add an asymmetric time smearing for small times due to the finite ion deposition density along the track.

We then fixed the values of n and m at 2 and 4.5 respectively, and assumed that changes to the drift velocity function could be characterized by a changing value of V_0 or b. By assuming that the maximum drift distance, $D_{\max}$, occurs at time $T_{\max}$, we are able to express b as follows:

$$b = \frac{D_{\max} - V_0 T_{\max}}{1 - n/m}.$$

So we have parameterized the drift distance in terms of two fundamental parameters, V_0, the saturated drift velocity, and $T_{\max}$, the maximum drift time.

Our calibration strategy relies on assuming that changes to the drift velocity correlation can be adequately described as a change to a single parameter, $T_{\max}$, which we must determine and periodically update in a calibration file.

2.4. Measuring T_{max}

We plan to use three methods to measure $T_{\max}$. The first is to allow $T_{\max}$ to be an adjustable parameter in a fit of the D vs. T data. The second is to fit the large-time edge of the drift-time histogram. The third is to measure $T_{\max}$ in a separate test chamber (at the same pressure, gas mixture and voltage as the actual chambers) by shining an UV laser onto field wire surfaces [5]. The ionization from the wire surface far exceeds the laser's ionization of the gas itself, so the recorded time spectrum is a direct measure of $T_{\max}$.

The first method is biased because the current value of D depends upon the parameters of the correlation function used to calculate D from T. This procedure is thus inherently an iterative one. The second and third methods yield values for $T_{\max}$ which *do not* depend upon track-fitting. However, the second method (fitting the trailing edge of the drift time histogram) will require a substantial amount of analysis to convert raw TDC readings into actual drift times because we will have a common-stop system with a trigger formation time jitter on the order of 40 ns. We have studied the laser calibration method and find that it yields results which are consistent with the other two methods, and has the advantage that it can be done independently of the data analysis.

Using a small one-cell test chamber we have obtained the time spectrum for pulses in which the electrons were photoemitted from a field wire surface. Fig. 5 is a time histogram from a cosmic-ray run on the one-cell chamber. Superimposed upon the continuous distribution of times obtained from the cosmic rays are two sharp peaks. The first is the time recorded from a diode situated near the chamber which was illuminated by the laser light and corresponds to the time at which the laser struck the wire. The second peak corresponds to electrons emitted from the field wires. The

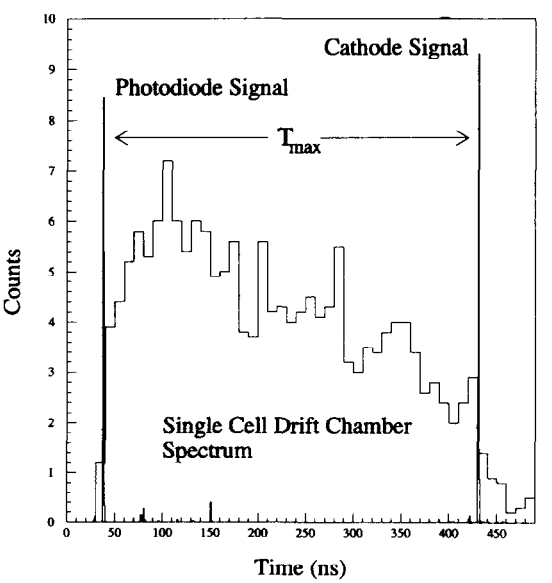

Fig. 5. Raw time histogram: cosmic ray run with laser peaks superimposed.

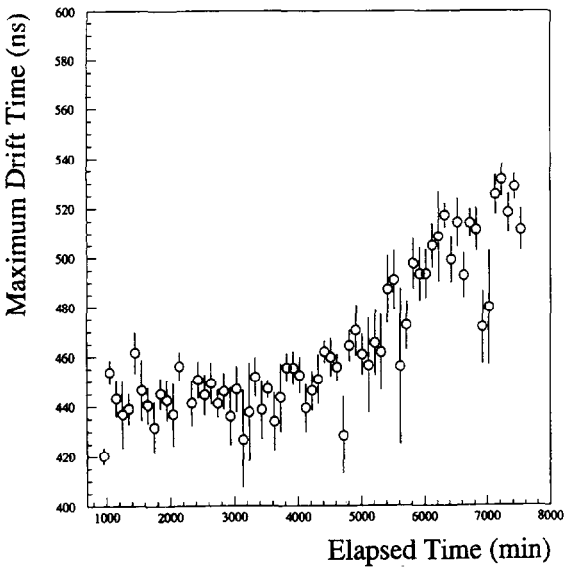

Fig. 6. Fitted value of T_{max} versus time of day.

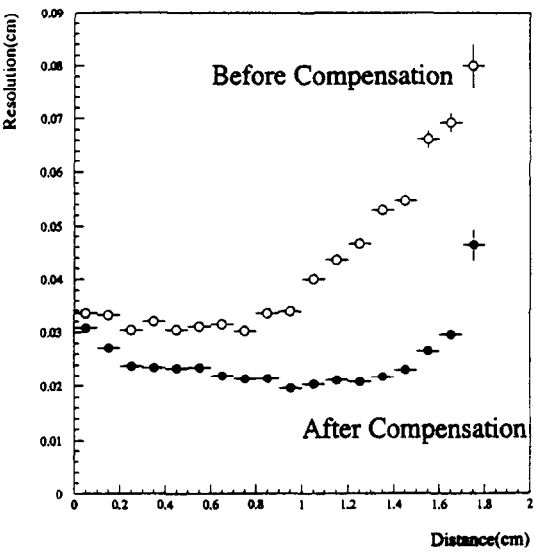

Fig. 7. Resolution versus D (before and after correction for changing T_{max}).

diode gives a prompt signal, so we have added one time offset to the two laser peaks in order to align the diode peak with the leading edge of the cosmic ray distribution. Note that the time difference between the peaks is the same as the overall time spread of cosmic-ray events, indicating that the laser pulsing method correctly measures the parameter T_{max}.

2.5. Environmental compensation

Changing environmental conditions affect the drift velocity, and thus the parameter T_{max}. As an example, Fig. 6 shows the change in the fitted value of T_{max} (trailing edge method) versus elapsed time for a 4-day data run. Notice that after 4000 min the value of T_{max} begins to change significantly. Our strategy for maintaining the drift velocity calibration is straightforward: measure T_{max} and update its value in the calibration file. Fig. 7 shows our results. We show the average residual between tracks and individual hits plotted versus the distance of the track from the wire. The open circles represent the residual distribution for the large-elapsed-time portion of the run, using a D–T function which gave good resolution ($\approx 200\ \mu m$) for the early part of the run. The resolution had clearly deteriorated. The solid circles represent the residuals obtained when the D–T function was corrected for the changing values of T_{max} shown in Fig. 6.

This is our primary result: by measuring and adjusting a single parameter (T_{max}) we are able to keep the drift chambers calibrated in spite of changing environmental conditions.

Acknowledgements

We thank Professor Rory Miskimen, University of Massachussetts, Amherst, for bringing to our attention the possibility of using a laser to induce photo-emission from field wires. We thank Stan Majewski and his detector development group at CEBAF for assistance in data-taking and for helpful discussions. We would also like to thank Elton Smith for loaning us the laser used in these tests, and for helping with the set-up of the measurement.

References

[1] Conceptual Design Report: Basic Experimental Equipment, CEBAF (April 1990).
[2] F.J. Barbosa et al., Nucl. Instr. and Meth. A 323 (1992) 191.
[3] GARFIELD has been developed at the University of Mainz by R. Veenhof and revised by M. Guckes and K. Peters. See HELIOS note 154 (1986).
[4] Due to the discrete ionization along a track, times are asymmetrically smeared to larger values for tracks near the sense or field wires. This effect steepens the slope for $T = 0$ and flattens it for $T = T_{max}$. We correct for this effect in our fitting procedure.
[5] We first learned of this procedure from R. Miskimen, U. Massachussetts, Amherst; private communication.